

Idealized Annually Averaged Macroturbulent Hadley Circulation in a Shallow-Water Model

ORI ADAM AND NILI HARNIK

Department of Geophysical, Atmospheric and Planetary Sciences, Tel Aviv University, Tel Aviv, Israel

(Manuscript received 1 March 2012, in final form 7 June 2012)

ABSTRACT

The interaction of midlatitude eddies and the thermally driven Hadley circulation is studied using an idealized shallow-water model on the rotating sphere. The contributions of the annually averaged differential heating, vertical advection of momentum from a stationary boundary layer, and the gross effect of eddies, parameterized by Rayleigh damping, including a hemispherically asymmetric damping, are examined at steady state.

The study finds that the relative dominance of eddies, as quantified by the local Rossby number, is predicted by an effective macroturbulent Hadley circulation Prandtl number P_r . In addition, viscous solutions of the Hadley circulation width and strength, subtropical jet amplitude, and equator-to-pole temperature difference scale as deviations from the respective inviscid solutions.

Semianalytic solutions for the steady circulation are derived in the limit of weak eddy dominance (small P_r) as deviations from the respective inviscid solutions. These solutions follow a three-region paradigm: weak temperature gradient at the ascending branch of the Hadley circulation, monotonically decreasing angular momentum at the descending branch, and modified radiative–convective equilibrium at the extratropics. Using the three-region solutions, scaling relations found in the full solutions are reproduced analytically. The weak eddy-dominance solutions diverge from the full solutions as P_r increases and may become invalid for $P_r > 1$ due to the breakdown of the three-region global circulation structure.

The qualitative predictions of the response of the Hadley circulation to heating based on the weak eddy-dominance solutions and P_r are in agreement with the findings of more complex models and the observed atmosphere.

1. Introduction

The Hadley circulation (HC) is a central element of Earth's climate, transporting heat and momentum poleward and affecting the extent of the wet tropical and dry subtropical regions, and the properties of the midlatitude baroclinically unstable region. Understanding how the extent of the wet and dry regions, the HC strength (HCS), and the properties of the subtropical jets respond to variations of external parameters is therefore critical for understanding Earth's climate.

Recent studies show fundamental discrepancies between the predictions of comprehensive global circulation models (GCMs) and observations of the HC width and strength (Mitas and Clement 2005; Johanson and Fu

2009). These discrepancies could result from the shortcomings of observational products (Santer et al. 2005), hydrological cycle parameterization (Held and Soden, 2006), or inherent sensitivity due to nonmonotonic dependence on heating (Levine and Schneider 2011). This highlights the need for improved understanding of the dynamics of the HC in the presence of eddies.

Outside the deep tropics, the mean meridional circulation momentum and heat fluxes are dominated by eddies. Eddies, however, are not necessary for the maintenance of the HC. Schneider (1977) has shown that an HC forms in the limit of vanishing viscosity (the so-called nearly inviscid limit) if advection of zonal momentum is not neglected. Following Schneider (1977), Held and Hou (1980, hereafter HH) argued that in the limit of vanishing viscosity, the steady global circulation divides into two regions: a tropical thermally driven HC, in which angular momentum is conserved; and an extratropical region in radiative–convective equilibrium, in which the meridional wind vanishes. By requiring that (i) the heating at the

Corresponding author address: Ori Adam, Department of Geophysical, Atmospheric and Planetary Sciences, Tel Aviv University, Tel Aviv 69978, Israel.
E-mail: ori.adam@live.com

ascending branch is balanced by the cooling at the descending branch of the HC, (ii) the temperature field is continuous, and (iii) zonal winds at the surface are negligible relative to the winds aloft, the extent of the HC and the temperature and velocity fields can be calculated explicitly. For annually averaged heating, their resulting inviscid HC had a similar extent, weaker circulation strength, and stronger subtropical jets than the observed zonally and annually averaged atmosphere. These angular momentum-conserving (AMC) solutions of HH were extended to off-equatorial heating by Lindzen and Hou (1988) and time-dependent forcing by Fang and Tung (1999).

The weak horizontal temperature gradients characterizing the tropics can also be used as a simplifying assumption in dynamical models of the HC (e.g., Sobel et al. 2001). Satoh (1994) and Fang and Tung (1996) have shown that the HC width can be determined as the extent of the region in which temperature may be assumed uniform. The physical motivation for this assumption is that if convection is assumed to occur at a thin intertropical convergence zone, then the temperature at this zone constrains the temperature at the rest of the cell in the inviscid limit (cf. Emanuel et al. 1994).

Axisymmetric nearly inviscid theory poorly predicts the atmospheric circulation outside the deep tropics, both in observations and in eddy-permitting models (e.g., Schneider 2006). Existing eddy-mean flow interaction theory on the global scale is mostly restricted to sophisticated, highly parameterized models. A simple theory of the general circulation in which eddies and the thermal driving of the circulation play comparable roles in determining the properties of the HC does not exist (cf. Schneider 2006; Pfeffer 1981; Becker et al. 1997; Kim and Lee 2001).

Held (2000) suggested a simple principle that determines the HC width in the presence of eddies: the HC ends where the thermally driven jet either first becomes unstable or reaches the latitude predicted in the nearly inviscid limit. To obtain an explicit scaling relation for the HC boundary, which requires an explicit solution for the tropical region, Held assumed angular momentum conservation, even though this assumption does not hold in the presence of eddies. Despite this inconsistency, there is some evidence that the edge of the HC scales as Held suggested in GCMs of varying complexity (e.g., Lu et al. 2007; Walker and Schneider 2006; Kang and Lu 2012).

Shallow-water models (SWMs) provide a simple platform for modeling the upper branch of the HC (e.g., Polvani and Sobel 2002 and references herein). Indeed, the angular momentum-conserving solutions of HH and Lindzen and Hou (1988), derived for the upper branch of a Boussinesq fluid on the rotating sphere, are identical

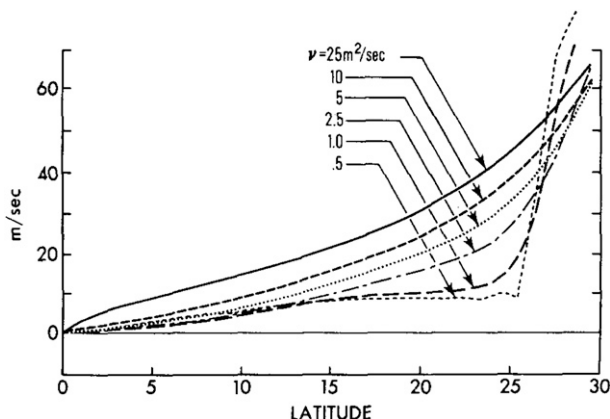


FIG. 1. Adapted from Fig. 6 of HH. Dependence on latitude of the difference from the predicted angular momentum level (divided by Earth's radius a), $\Omega a \sin^2(\phi) - u \cos(\phi)$, at the top of the troposphere, where Ω is the rotational frequency of Earth. Shown are results at steady state for various values of vertical diffusion ν .

to solutions derived using a shallow-water model on the rotating sphere (Adam and Paldor 2009, 2010a). Similarly, Polvani and Sobel (2002) derived solutions of the upper branch of the HC based on a shallow-water model by assuming a weak temperature gradient throughout the HC. Unlike Satoh (1994) and Fang and Tung (1996), however, in which both angular momentum and temperature are assumed uniform, the weak temperature gradient solutions of Polvani and Sobel (2002) do not require the conservation of angular momentum and thus permit parameterized eddy damping. While neglecting the temperature gradient outside the ascending branch of the HC is not strictly justifiable, Polvani and Sobel (2002) showed that the weak temperature gradient solutions are in good agreement with the steady states of their model. More importantly, the assumption of a weak temperature gradient holds in the presence of eddies, making solutions based on this assumption unique, in that they represent the only known case in which semianalytic solutions of the HC width and strength can be obtained with parameterized eddy damping.

Inspection of the numerical solutions of the model employed by HH, Lindzen and Hou (1988), and Fang and Tung (1999) (Boussinesq fluid allowed to vary in latitude and height on a rotating sphere, bounded by a rigid lid) reveals that the ascending and descending branches of the HC differ considerably. As shown in Fig. 1, adapted from HH, even at the lowest viscosity for which stable solutions were obtained, angular momentum is conserved at the subtropics but is not conserved at the deep tropics. As suggested by HH and Lindzen and Hou (1988), strong vertical mixing prevents the conservation of angular momentum at the ascending branch of the HC. Schneider (1984, 1987) suggested that explicit

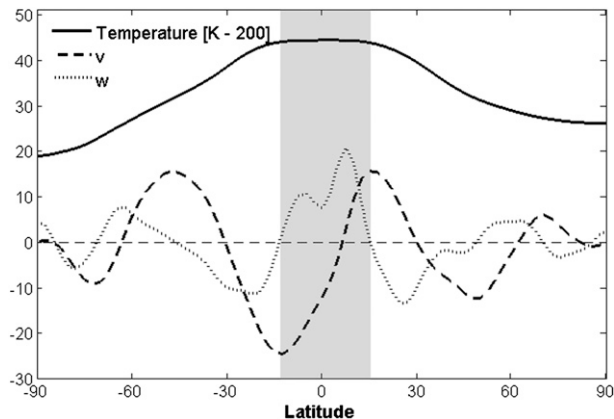


FIG. 2. The dependence on latitude of the annually, zonally, and vertically (200–500-mb levels) averaged temperature ($K-200$, solid), meridional (dashed) and vertical (dotted) winds [National Centers for Environmental Prediction–National Center for Atmospheric Research (NCEP–NCAR) reanalysis, long-term monthly averages for the years 1979–2010]. For presentational clarity, temperature is shown as $T - 200$ K, and the meridional and vertical winds are brought to scale by using units of $1/50$ and $1/1000$ m s^{-1} , respectively. The ascending branch ($w > 0$) of the annually averaged Hadley circulation, subtended by the poleward maxima in the meridional wind and characterized by a weak temperature gradient, is shaded. A horizontal zero line (dashed) is added for reference.

inclusion of vertical momentum fluxes may be considered as a different nearly inviscid limit in better agreement with observations.

Adam and Paldor (2009) noted that while vertical advection of momentum (VAM) prevents angular momentum conservation in the ascending branch of the HC, a weak temperature gradient assumption is valid in this region. Vertical advection of momentum, however, does not affect the descending branch of the HC in the inviscid case, allowing for conservation of angular momentum there. Thus, they suggested a three-region paradigm of the mean meridional circulation for the steady, inviscid circulation: weak temperature gradient at the ascending branch of the HC, angular momentum conservation at the descending branch, and radiative–convective equilibrium at the extratropics. Adam and Paldor (2009) derived semianalytic solutions for the axisymmetric upper branch of the HC in the presence of vertical advection of momentum from a stationary boundary layer, which reproduce the angular momentum profile shown in Fig. 1.

Support for a three-region paradigm is found in the zonally and annually averaged atmosphere. The annually and zonally averaged upper troposphere can be described as being barotropic at the ascending branch of the HC and polar regions, and baroclinic at midlatitudes. Figure 2 shows the dependence on latitude of the vertical average between the 500- and 200-mb levels of the annually and

zonally averaged temperature (solid), meridional wind (dashed), and vertical wind (dotted). The annually averaged ascending branch of the HC is thus very clearly observed as a positive vertical velocity (w) region, bounded by the maxima in the poleward meridional wind and characterized by a weak temperature gradient.

Thus, while inviscid models poorly predict the properties of simulated and observed HC, a three-region approach may still be justified in studying the macroturbulent HC. In the limit of weak macroturbulence, a weak-temperature-gradient approximation is still valid at the ascending branch of the HC, while angular momentum conservation at the descending branch of the HC and radiative–convective equilibrium at the extratropics are modified relative to their respective inviscid states.

In this work we seek to study general aspects of the effect of eddies on the HC by (i) assuming a three-region structure of the mean meridional circulation; (ii) using simplified eddy parameterization; (iii) comparing and relating the inviscid and viscous (i.e., eddy permitting) steady states of the simplified model; and (iv) establishing an analytic framework for deriving semianalytic solutions of the steady states of the viscous system, which is applicable to general forms of eddy parameterization. We therefore employ a shallow-water model in which vertical advection of momentum and eddy momentum flux divergence are given simplified parameterizations.

In section 2 we present the model. In section 3 we review the known inviscid solutions of the model. In section 4 we report the results of a wide parameter sweep of the steady states at long times of the time-dependent model and compare these steady states with the respective inviscid solutions. In section 5 we derive semianalytic solutions for the steady viscous states as small deviations from the inviscid solutions, followed by a summary and discussion in section 6.

2. Model equations

To model the upper branch of the HC, we employ a differentially heated SWM on the rotating sphere, with vertical advection of momentum from a stationary boundary layer and Rayleigh damping. This model differs from the one described in Adam and Paldor (2010b) and Shell and Held (2004) only in its representation, which better serves the semianalytic solutions presented in section 5. A similar model is discussed in Held and Hoskins (1985). For clarity, the model representation is derived below.

The shallow-water equations (e.g., Gill 1982) on the spherical Earth [with radius a , and latitude (ϕ) and longitude (λ) coordinates] rotating about its polar axis (frequency Ω but no centrifugal acceleration) with a

source of mass (height) Q , vertical advection of momentum from a stationary bottom layer and Rayleigh damping are given by

$$\frac{Dv}{Dt} = -\left(2\Omega + \frac{u}{a \cos\phi}\right)u \sin\phi - \frac{g}{a} \frac{\partial h}{\partial \phi} - \left(\frac{IQ}{h} + r\right)v, \quad (1a)$$

$$\frac{Du}{Dt} = \left(2\Omega + \frac{u}{a \cos\phi}\right)v \sin\phi - \frac{g}{a \cos\phi} \frac{\partial h}{\partial \lambda} - \left(\frac{IQ}{h} + r\right)u, \quad (1b)$$

$$\frac{\partial h}{\partial t} + \frac{1}{a \cos\phi} \left[\frac{\partial}{\partial \lambda}(hu) + \frac{\partial}{\partial \phi}(hv \cos\phi) \right] = Q, \quad (1c)$$

where $D/Dt = \partial/\partial t + [u/(a \cos\phi)](\partial/\partial \lambda) + (v/a)(\partial/\partial \phi)$ denotes the material (total, Lagrangian) derivative in spherical coordinates; g is the gravitational constant; r is the Rayleigh coefficient of damping; u and v denote the longitudinal and meridional velocity components, respectively; and h denotes the thickness of the free troposphere. The source is given as Newtonian relaxation to a prescribed radiative–convective equilibrium height h_f as follows:

$$Q = \frac{h_f - h}{\tau}, \quad (1d)$$

where

$$h_f = H_0 + \Delta_H \left[\frac{1}{2} - (\sin\phi - \sin\phi_0)^2 \right]. \quad (1e)$$

Here, τ is a constant atmospheric thermal relaxation time (typically 2–3 weeks), H_0 is the tropospheric height scale (~ 10 km), Δ_H , the equator-to-pole temperature (height) difference (EPTD ~ 3 km) at radiative–convective equilibrium, and ϕ_0 is the latitude of maximal heating. This prescribed form of h_f follows the upper branch of the radiative forcing used by HH for heating centered at the equator ($\phi_0 = 0$, equinoctial case) and Lindzen and Hou (1988) for off-equatorial heating ($\phi_0 \neq 0$). Following Schneider (1987), the term h_f/τ is ascribed to the contributions of solar and latent convective heating, and $-h/\tau$ is ascribed to longwave radiative cooling.

The heaviside function I is given by

$$I(Q) = \begin{cases} 0; & Q \leq 0 \\ 1; & Q > 0 \end{cases}, \quad (1f)$$

so that momentum is conserved locally when mass from the stationary bottom layer enters the upper layer.

Equations (1a)–(1f) are nondimensionalized using the following scales: u and v on Ωa , t , τ ; $1/r$ on $1/\Omega$; and h and h_f on H_0 . Absolute angular momentum,

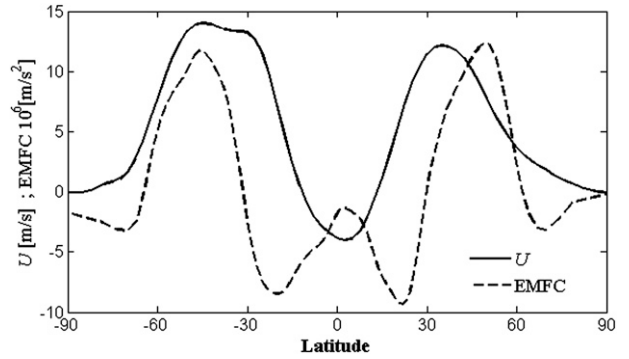


FIG. 3. Long-term annual and zonal mean of the zonal wind [$U = u \cos(\phi)$, solid], and the sum of transient and stationary EMFC (dashed), averaged between the 850- and 200-mb levels. Data are taken from National Oceanic and Atmospheric Administration (NOAA)/NCEP for the years 1990–2010.

$M = \cos\phi a(\Omega a \cos\phi + u)$, is scaled by Ωa^2 . To simplify the subsequent analysis, we make the following substitutions in system (1): M for u , $V = v \cos\phi$ for v , and $\mu = \sin\phi$ for ϕ . Axial symmetry is introduced by setting the longitudinal derivative equal to zero. Using $(\cdot)'$ to denote $\partial/\partial \mu$, these substitutions yield the following non-dimensional system:

$$\frac{\partial V}{\partial t} = -VV' - \frac{\mu(V^2 + M^2)}{1 - \mu^2} + (1 - \mu^2)(\mu - \alpha h') - \left(\frac{IQ}{h} + r\right)V \quad (2a)$$

$$\frac{\partial M}{\partial t} = -VM' - \left(\frac{IQ}{h} + r\right)(M - 1 + \mu^2) \quad (2b)$$

$$\frac{\partial h}{\partial t} = -(Vh)' + Q \quad (2c)$$

$$Q = \frac{h_f - h}{\tau}, \quad (2d)$$

where

$$h_f = 1 + \Delta_h \left[\frac{1}{2} - (\mu - \mu_0)^2 \right]; \quad \text{and} \quad (2e)$$

$$\alpha = \frac{gH_0}{\Omega^2 a^2} \quad (2f)$$

is the planetary Burger’s number with a typical value of 0.45. Since g , Ω and a may be assumed fixed in Earth’s atmosphere, variations in α are attributable to H_0 , which we also interpret as the mean global temperature. Similarly, we attribute Δ_h to the differential heating of the sun.

We interpret r as modeling the gross effect of eddies on the HC. Figure 3 shows a long-term annual mean of

the zonally and vertically averaged $U = u \cos(\phi)$ (solid) and sum of transient and stationary eddy momentum flux convergence (EMFC, dashed; cf. Fig. 1 in Lee 1999). Eddy parameterization using Rayleigh damping is therefore in agreement with the observed poleward momentum flux at midlatitudes but in disagreement with the observed equatorward momentum fluxes in the deep tropics and polar regions. From Fig. 3, we find that the typical value of U/EMFC is on the order of 1000 days, which is much longer than the typical eddy-mean flow response time of 1 week at midlatitudes (Lorenz and Hartmann 2001). This suggests that r represents the damping rate of the entire tropical circulation, which this model implies is much longer.

Eddy parameterizations more complex than Rayleigh damping have been shown to capture some of the basic features of seasonal climatology (e.g., Schneider 1984, Sobel and Schneider 2009). In this work we neglect the momentum fluxes associated with equatorial waves and consider only the effect of midlatitude momentum fluxes on the HC. However, since EMFC in the deep tropics and polar regions is small relative to EMFC at midlatitudes, and since this work is of a qualitative nature, we justify the parameterization of EMFC using simple Rayleigh damping for its mathematical and conceptual simplicity (e.g., Shell and Held 2004; Polvani and Sobel 2002).

Further discussion of the physical interpretation of the SWM can be found in Adam and Paldor (2009, 2010a).

3. Inviscid steady states

In this section we briefly describe the known semi-analytic solutions of the inviscid SWM for the case of annually averaged (equinoctial) heating ($\mu_0 = 0$) with vertical advection of momentum (Adam and Paldor 2009) and without it (HH). We will refer to these known solutions in the following sections, and in particular to their predictions of the HC strength and width.

a. AMC solutions

For the case of the inviscid SWM ($r = 0$) at steady state, without vertical advection of momentum ($I = 0$), Eq. (2b) becomes

$$VM' = 0, \quad (3)$$

so that the SWM has only two steady states: uniform- M steady state, given by

$$V = \frac{\int (h_f - h) d\mu}{\tau h}, \quad (4a)$$

$$h = h_0 + \frac{1}{2\alpha} \left(\mu^2 - \frac{\overline{M}^2}{1 - \mu^2} \right), \quad (4b)$$

$$M = \overline{M}, \quad (4c)$$

where \overline{M} and h_0 are constants; and a radiative-convective equilibrium ($V, Q = 0$) steady state, given by

$$V = 0, \quad (5a)$$

$$h = h_f, \quad (5b)$$

$$M = (1 - \mu^2) \sqrt{1 - \frac{\alpha h'_f}{\mu}}. \quad (5c)$$

Since neither radiative-convective equilibrium nor uniform M are physically realistic as global steady states, the circulation divides into a tropical uniform- M region and an extratropical radiative-convective equilibrium region (cf. HH; Adam and Paldor 2009, 2010a).

Requiring conservation of mass and continuity of h , and assuming that the zonal velocity vanishes at the equator, the latitude separating the two regions and marking the polar boundary of the HC (μ_H) is obtained by the roots of

$$\frac{\overline{M}^2}{1 + 2R_T} \left[\frac{\mu_H}{1 - \mu_H^2} - \frac{1}{2} \ln \left(\frac{1 + \mu_H}{1 - \mu_H} \right) \right] - \frac{2}{3} \mu_H^3 = 0. \quad (6a)$$

A small angle approximation then yields

$$\phi_H \simeq \sqrt{\frac{5}{3}} R_T, \quad (6b)$$

where $R_T = \alpha \Delta_h$ is the thermal Rossby number. These are the well-known angular momentum-conserving solutions of HH, in which due to Hide's theorem, $\overline{M} = 1$ (i.e., u vanishes at the equator; cf. HH; Adam and Paldor 2009).

Since $Q = (h_f - h)/\tau$ changes sign at the polar boundary of the heated region (ascending branch), from Eq. (4) we find that at this latitude, denoted as μ_A , Vh reaches its maximum. Using Eq. (4) and the continuity of h , we get

$$\mu_A = \sqrt{1 - \frac{\overline{M}^2}{1 + 2R_T} \frac{1}{(1 - \mu_H^2)}}. \quad (7)$$

We refer to the value of the mass flux at this latitude as the HCS, defined as

$$\text{HCS} = Vh|_{\mu=\mu_A}. \quad (8)$$

While some qualitative differences exist between alternative definitions of the HC strength (e.g., Levine and

Schneider 2011), we find the above-mentioned form suitable for this study.

b. Inviscid model with VAM

The steady states of the SWM for the case of the inviscid ($r = 0$) model with vertical advection of momentum follow a three-region paradigm where each region is unique to $\text{sign}(Q)$: a radiative–convective equilibrium ($Q = 0$) extratropical region given by Eq. (5), a subtropical uniform- M cooling ($Q < 0$, descending HC branch) region given by Eq. (4), and a tropical heating ($Q > 0$, ascending HC branch) region characterized by a uniform height \bar{h} (i.e., weak temperature gradient), given by

$$h = \bar{h} = 1 + \Delta_h \left(\frac{1}{2} - \mu_A^2 \right) \tag{9a}$$

$$V = \frac{\int (h_f - \bar{h}) d\mu}{\tau \bar{h}} = \frac{\Delta_h}{\tau} \frac{\mu_A^2 \mu - \frac{1}{3} \mu^3}{1 + \Delta_h \left(\frac{1}{2} - \mu_A^2 \right)} \tag{9b}$$

$$M = 1 - \frac{\int (h_f - \bar{h}) \mu^2 d\mu}{\int (h_f - \bar{h}) d\mu} = 1 - \frac{\mu_A^2 \mu^2 - \frac{3}{5} \mu^4}{3\mu_A^2 - \mu^2}. \tag{9c}$$

Requiring conservation of mass and continuity of h , μ_A and μ_H are found by the roots of

$$\left(1 - \frac{1}{5} \mu_A^2 \right)^2 = (1 + 2R_T)(1 - \mu_A^2)(1 - \mu_H^2) \tag{10a}$$

and

$$\begin{aligned} & \frac{\left(1 - \frac{1}{5} \mu_A^2 \right)^2}{1 + 2R_T} \left\{ \frac{\mu_H - \mu_A}{1 - \mu_H^2} - \frac{1}{2} \ln \left[\frac{(1 + \mu_H)(1 - \mu_A)}{(1 - \mu_H)(1 + \mu_A)} \right] \right\} \\ & = \frac{\mu_A^3}{3} \left(\frac{1 + 6R_T}{1 + 2R_T} \right) + \frac{2\mu_H^3}{3} - \mu_H^2 \mu_A. \end{aligned} \tag{10b}$$

From Eq. (10a), a small angle approximation yields

$$\mu_H \simeq \sqrt{2R_T/(1 + 2R_T)}. \tag{11}$$

The dependence of μ_H and μ_A on R_T for both VAM (solid) and AMC (dashed) solutions is shown later (see the left panel of Fig. 8; cf. Fig. 2 in HH; Fig. 9 in Adam and Paldor 2009).

Note that the vertical advection of momentum solutions of Adam and Paldor (2009) assume a weak temperature

gradient only at the ascending branch of the HC, and not throughout the entire HC as was done by Polvani and Sobel (2002). In addition, the main difference of the vertical advection of momentum solutions from those of Polvani and Sobel (2002) and HH is that they offer a dynamic definition of the tropics, in agreement with the observed zonally averaged atmosphere, that is, the equatorial ascent region, characterized by a weak temperature gradient and bounded by the latitude of maximal poleward mass flux.

Since Vh is maximal at μ_A , and since we also have $h(\mu_A) = h_f(\mu_A)$, from Eq. (9b) the HC strength is given by

$$\text{HCS} = Vh|_{\mu=\mu_A} = \frac{2 \Delta_h \mu_A^3}{3 \tau}. \tag{12}$$

Assuming that like μ_H , μ_A scales with $\sqrt{R_T}$, the HC strength in the inviscid case approximately scales with $R_T^{3/2} \Delta_h / \tau = \alpha^{3/2} \Delta_h^{5/2} / \tau$, which is the scaling found by HH [Eq. (18) in HH]. In the following section (Fig. 7) we show that the HC strength in the inviscid case scales nearly linearly with $R_T \Delta_h / \tau = \alpha \Delta_h^2 / \tau$.

4. Steady states of the viscous ($r > 0$) SWM

To study the effect of eddies, as parameterized by Rayleigh damping r , we begin by examining the steady states obtained by long time integrations of Eq. (2). Time integrations were performed using a staggered-grid (where h is staggered from V and M) leapfrog scheme with a Robert–Asselin time filter (temporal damping coefficient = 0.001), as described in Adam and Paldor (2009). A spatial resolution of 1000 meridional grid points, evenly spaced in μ , was used in the results shown below. This translates into a resolution of 0.01, 0.015, and 0.05° of latitude in the tropics, midlatitudes, and polar regions, respectively.

Taking advantage of the simplicity of the SWM, we performed a numerical parameter sweep (~1000 model runs) of the steady solutions at long times of the time-dependent equations of the SWM for a wide range of parameter values. It is readily shown that if t is scaled by the thermal relaxation time τ , Eq. (2) can be represented by an effective Rayleigh coefficient of damping $r\tau$ [cf. Adam and Paldor (2010b) and Fang and Tung (1997) for the scaling of τ in the inviscid case]. It is therefore the product of r and τ (i.e., ratio of thermal and effective eddy-damping time scales) that affects solutions at steady state. This will also become evident in the subsequent analysis. We therefore performed a parameter sweep for the parameter ranges: $\alpha = 0.15$ – 1.7 , $\Delta_h = 2/15$ – $2/3$ ($R_T = 0.1$ – 0.225), and $r\tau = 0.001$ – 1 . These parameter ranges represent the physically realistic extremities of the model

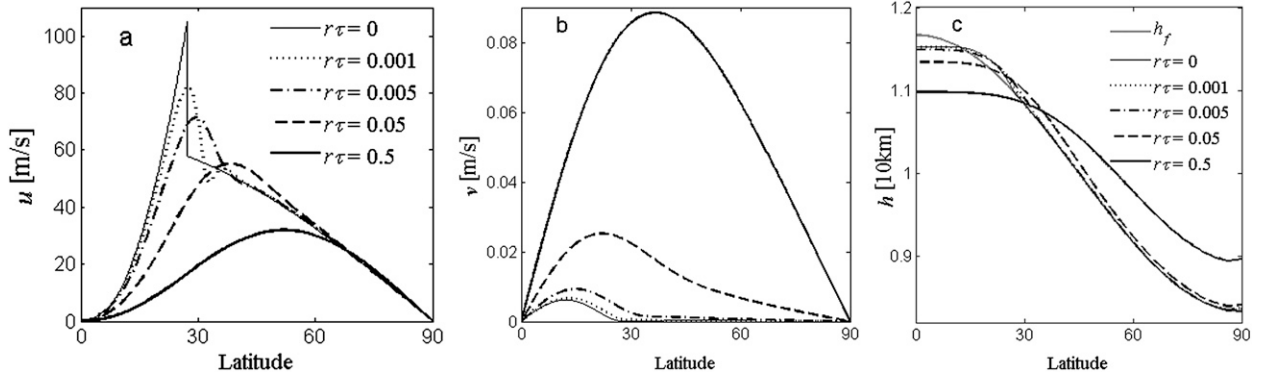


FIG. 4. (a) Zonal velocity u (m s^{-1}), (b) meridional velocity v (m s^{-1}), and (c) height (10 km), at steady state for $\alpha = 0.45$, $\Delta_h = 1/3$, $r\tau = 0$ (VAM solutions), 0.001, 0.005, 0.05, and 0.5. These values correspond to $R_T = 0.15$ and $P_r = 0, 0.02, 0.1, 1, \text{ and } 10$. The radiative-convective equilibrium height is shown in gray in (c) for reference.

parameters α and Δ_h for Earth, and a wider range of $r\tau$ values.

Figure 4 presents the steady states for the zonal wind (Fig. 4a), meridional wind (Fig. 4b), and height (Fig. 4c) at long times for $\alpha = 0.45$, $\Delta_h = 1/3$ ($R_T = 0.15$), and $r\tau = 0$ (VAM solutions), 0.005, 0.05, and 0.5 (cf. Figs. 5 and 7 in HH).

Several robust features of the steady states of the SWM emerge from the wide parameter sweep, which we also derive analytically in the following section.

The local Rossby number, defined as

$$\text{Ro} = -\zeta/f = 1 + M'/\mu \quad (13)$$

(where ζ is relative vorticity and f is the Coriolis parameter), can be perceived as a measure of the degree to which angular momentum is conserved meridionally (e.g., Schneider 2006). Since in the inviscid case angular momentum is conserved in the descending branch (where $Q < 0$), the value of Ro may be used to quantify the dominance of eddy momentum fluxes there. As shown in Fig. 5, Ro approximately depends on a single parameter, which represents the competition between the differential heating of the sun (which drives the HC and subtropical jets) and eddy momentum fluxes (which feed on the energy of the subtropical jets). This ratio, denoted by P_r , can be thought of as an effective HC Prandtl number, which relates eddy and thermal driving of the HC on the rotating sphere, is defined as

$$P_r = \frac{r\tau}{\alpha\Delta_h^2} = \frac{r\tau}{R_T\Delta_h} = \frac{\Omega^2 a^2 r\tau}{gH_0\Delta_h^2}. \quad (14)$$

Shown as dots are Ro values calculated at μ_A for the entire parameter sweep (other representations of Ro, e.g., the mean of Ro over the entire descending branch

region, yield similar dependence on P_r). A clear separation of the steady states into three regimes is observed:

Weak eddy dominance: $\text{Ro} \sim 1$, $P_r \rightarrow 0$

Intermediate eddy dominance: $0 < \text{Ro} < 1$, $P_r \sim 1$

Strong eddy dominance: $\text{Ro} \sim 0$, $P_r \gg 1$

The steady states shown in Fig. 4 for $r\tau = 0, 0.005, 0.05, \text{ and } 0.5$ correspond to $P_r = 0, 0.02, 0.1, 1, \text{ and } 10$, respectively.

The dependence of Ro on P_r shown in Fig. 5 predicts that Ro increases (i.e., eddy dominance decreases) in response to mean (α) and differential (Δ_h) heating, as

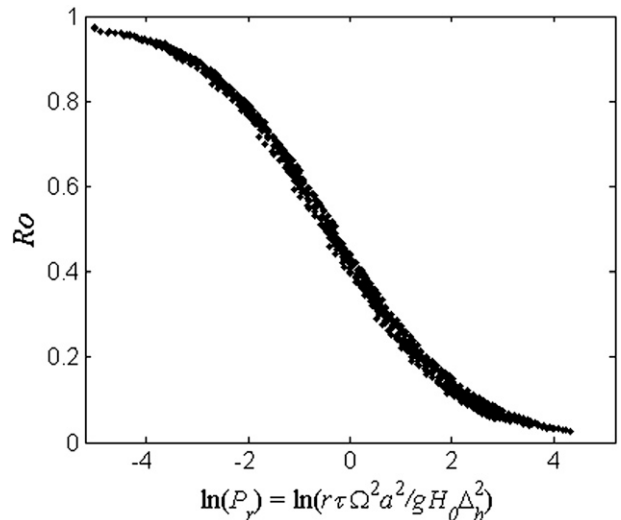


FIG. 5. The local Rossby number, $\text{Ro} = 1 + M'/\mu$, calculated at the polar boundary of the ascending branch of the Hadley circulation (μ_A), plotted against $\ln(P_r)$ ($P_r = r\tau/\Delta_h R_T$). Shown as dots are Ro values at steady state of the time-dependent SWM obtained by long time integrations for the parameter ranges: $\alpha = 0.15\text{--}1.7$, $\Delta_h = 2/15\text{--}2/3$ ($R_T = 0.1\text{--}0.225$), $r\tau = 0.001\text{--}1$.

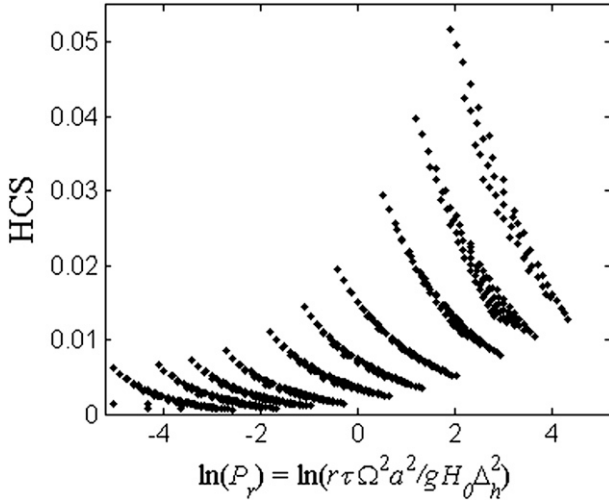


FIG. 6. Dependence of the nondimensional HCS on $\ln(P_r)$ ($P_r = r\tau/\Delta_h R_T$). Shown as dots are the values at steady state of the time-dependent SWM obtained by long time integrations for the parameter ranges: $\alpha = 0.15\text{--}1.7$, $\Delta_h = 2/15\text{--}2/3$ ($R_T = 0.1\text{--}0.225$), and $r\tau = 0.001\text{--}1$.

well as in response to a decreased rotation rate Ω . We further elaborate on the agreement of this dependence with existing theory and observations in the discussion (section 6).

We find that steady-state variables for $r > 0$ generally do not scale with P_r , as shown in Fig. 6 for the HC strength, for example. The different branches seen in Fig. 6

correspond to different values of r , with the HC strength increasing with r . The HC strength increases with $gH_0\Delta_h^2/\tau\Omega^3a^2$ within branches, as in the inviscid case. Accordingly, we find that when the HC strength and width are scaled by their respective value in the inviscid case (vertical advection of momentum solutions for $r = 0$ and same α , Δ_h , and τ), a dependence on P_r , very similar to that observed for Ro (Fig. 5) emerges.

The scaling of the HC strength in the inviscid case, for VAM (solid) and AMC (dashed) solutions, is shown in the left panel of Fig. 7 for the parameter ranges used in the parameter sweep. The dependence on P_r of the inverse of the HC strength, scaled by its respective inverse inviscid value (hereafter referring to VAM solutions) is shown in the right panel of Fig. 7. The similarity of the dependence of the scaled HC strength and Ro on P_r implies that it is the deviation from inviscid solution that scales with P_r , and that this deviation from inviscid solutions is closely associated with the level of eddy dominance.

A similar dependence on P_r is found for μ_A and μ_H . While in the inviscid case, μ_H denotes the latitude of both HC width and subtropical jet, this is no longer the case in the viscous case. If we assume a three-region structure at steady state (ascending branch, descending branch, and modified radiative–convective equilibrium regions), then we expect a transition region from the descending branch to a modified radiative–convective equilibrium poleward of the latitude of the subtropical

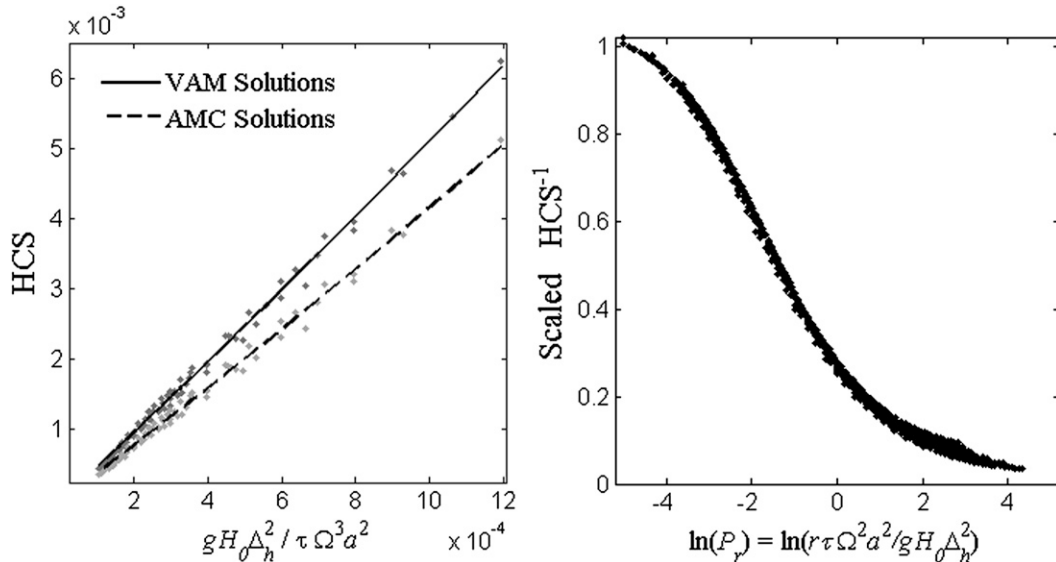


FIG. 7. (left) The smoothed scaling of the nondimensional HCS [$\text{HCS} = \max(Vh)$] for VAM solutions (solid) and AMC (dashed) solutions. Dots represent particular steady states. (right) The dependence of the ratio of HCS in the inviscid case and HCS for $r > 0$ (the inverse of the HCS for $r > 0$, scaled by the respective HCS in the inviscid case) on $\ln(P_r)$ ($P_r = r\tau/\Delta_h R_T$). Shown as dots are the values at steady state of the time-dependent SWM obtained by long time integrations for the parameter ranges: $\alpha = 0.15\text{--}1.7$, $\Delta_h = 2/15\text{--}2/3$ ($R_T = 0.1\text{--}0.225$), and $r\tau = 0.001\text{--}1$.

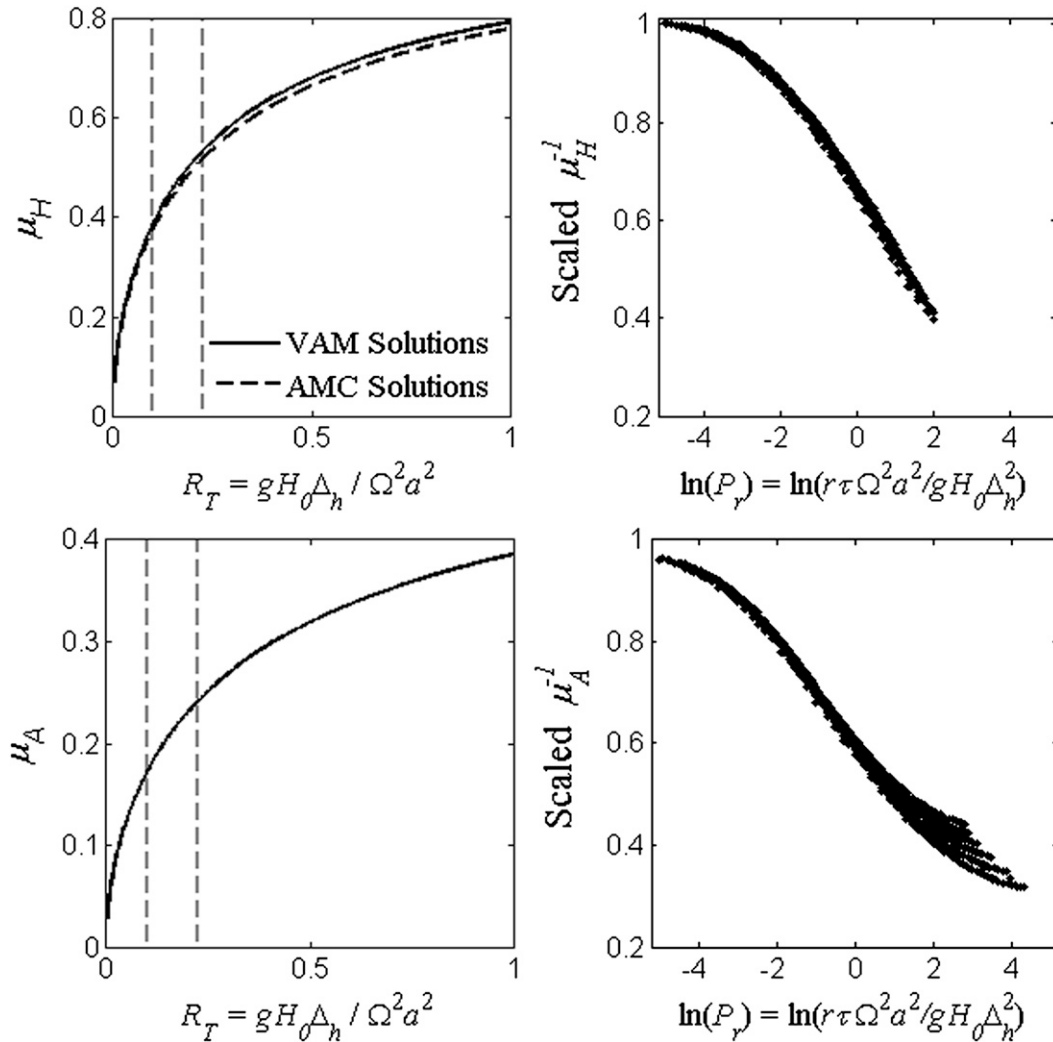


FIG. 8. (left) The dependence of (top) μ_H and (bottom) μ_A , on $R_T = \alpha\Delta_h$, for the inviscid ($r = 0$) VAM and AMC solutions. Vertical dashed lines indicate the range of R_T values of the viscous steady states shown in the right panels. Differences in the AMC and VAM solutions for μ_A in the left bottom panel are negligible. (right) The dependence of the (top) inverse of μ_H and (bottom) μ_A , scaled by the respective inviscid solution (VAM solutions for same α and Δ_h but $r = 0$) on $\ln(P_r)$ ($P_r = r\tau/\Delta_h R_T$). Shown as dots are the values at steady state of the time-dependent SWM obtained by long time integrations for the parameter ranges: $\alpha = 0.15$ – 1.7 , $\Delta_h = 2/15$ – $2/3$ ($R_T = 0.1$ – 0.225), and $r\tau = 0.001$ – 1 . Steady states for which $\mu_H = 1$, indicating a three-region separation cannot be assumed, are removed from the top right panel. Vertical dashed lines in the left panels indicate the range of R_T values of the viscous steady states shown in the right panels.

jet μ_{STJ} [latitude of $\max(U)$]. We therefore define μ_H as the latitude where the second derivative of the mass flux is maximal, poleward of the latitude of the subtropical jet: $\max(Vh)''|_{\mu \geq \mu_{\text{STJ}}}$. This definition is also valid in the inviscid case, where $\mu_H = \mu_{\text{STJ}}$. The left panels of Fig. 8 show the dependence of μ_H (top) and μ_A (bottom) on the R_T , in the inviscid case for VAM (solid) and AMC (dashed) solutions. The right panels of Fig. 8 show the inverse of μ_H (top) and μ_A (bottom), scaled by their respective inverse values in the inviscid case. Steady states for which $\mu_H = 1$, indicating that the assumption

of a three-region structure is not valid, are removed from the top panel. Similar to the HC strength, the resemblance of the dependence on P_r of the scaled inverse of μ_H and μ_A and Ro (Fig. 5) allows for associating the deviation from the inviscid solution with the level of eddy dominance. A similar dependence to that of μ_H is found for μ_{STJ} (not shown).

Thus, we observe that the deviation from values in the inviscid case of the HC strength, and the latitudes of the μ_H , the μ_A , and the μ_{STJ} increase with P_r at a rate that depends on the associated Ro regime. We also find in

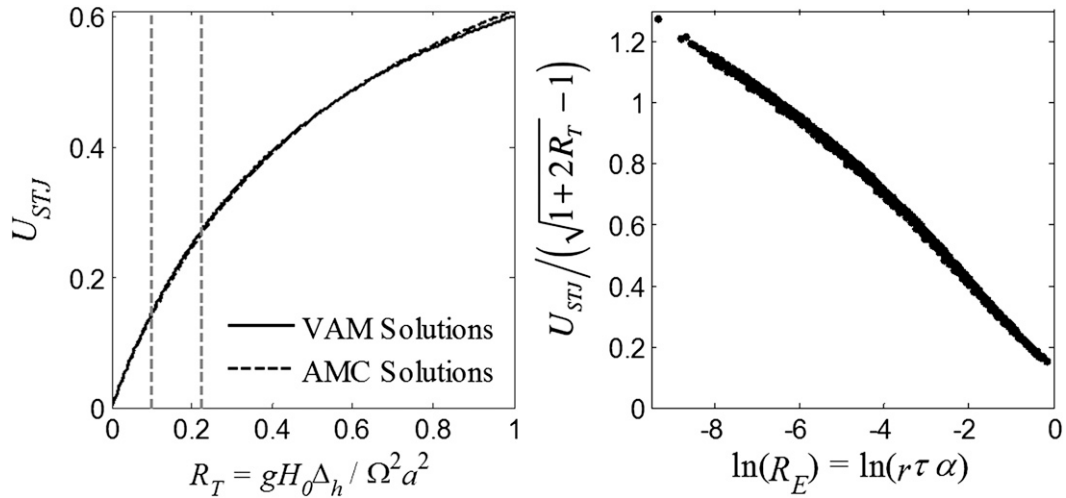


FIG. 9. (left) The dependence of U_{STJ} on R_T for VAM (solid) and AMC (dashed) solutions. (right) The dependence of U_{STJ} scaled by $(\sqrt{1 + 2R_T} - 1)$, on $\ln(R_E)$ ($R_E = r\tau\alpha$). Shown as dots are the values at steady state of the time-dependent SWM obtained by long time integrations for the parameter ranges: $\alpha = 0.15\text{--}1.7$, $\Delta_h = 2/15\text{--}2/3$ ($R_T = 0.1\text{--}0.225$), and $r\tau = 0.001\text{--}1$. Vertical lines in the left panel indicate the range of R_T values of the viscous steady states shown in the right panel.

our runs that for $P_r > 7.4$ ($Ro \sim 0.1$; e.g., Fig. 4, thick solid line), the viscous HC encompasses the entire globe, so that an extratropical modified radiative–convective equilibrium region ceases to exist. Such an extended HC is unlikely to occur on Earth but may be relevant for more slowly rotating planets.

From the left panels of Figs. 7 and 8, it is evident that in the inviscid case, both the HC width and strength monotonically increase in response to α and Δ_h (cf. Hou 1984; Hou and Lindzen 1992). We wish now to examine whether the addition of eddy damping (r) affects this monotonic behavior. The right panels of Figs. 7 and 8 suggest that a decrease in the HC strength or width in response to heating is allowed only at the intermediate or eddy-dominated Ro regime, and only if r is affected by the heating [i.e., $r = r(\alpha, \Delta_h)$] such that it decreases with mean or differential heating. In other words, while the inviscid response to heating is an increase in the HC strength, a sufficient decrease in the eddy-driven component of the circulation will lead to an overall decrease in the HC strength. Such a decrease in r can only occur for high enough P_r (low enough Ro), suggesting that for high enough P_r values, a nonmonotonic response of the HC strength to heating is allowed, while for low P_r values we expect a monotonic increase in the HC strength. A decrease of r with heating was shown, for example, by Levine and Schneider (2011, Figs. 4–6), who found a monotonic increase of Ro in response to heating, but a nonmonotonic response of the HC strength to heating, coupled to a nonmonotonic response of the eddy component of the HC. In their study, both the HC strength

and eddy component of the HC strength increased with mean temperature for temperatures below today’s climate conditions and then decreased as the mean temperature increased (and similarly, eddy kinetic energy, mean available potential energy, and eddy momentum flux convergence). Thus, we conclude that a non-monotonic response of the HC strength to heating is allowed if the effect of eddies depends on the heating.

We turn now to examine the amplitude of the subtropical jet. The subtropical jet amplitude in the inviscid case can be obtained from Eq. (5),

$$U_{STJ} = M - 1 + \mu_H^2 = (1 - \mu_H^2) (\sqrt{1 + 2R_T} - 1). \quad (15)$$

As shown on the left panel of Fig. 9, in the inviscid case the subtropical jet amplitude scales with R_T . We find that for $r > 0$, $U_{STJ} / (\sqrt{1 + 2R_T} - 1)$ monotonically (and close to linearly) decreases with $\ln(r\tau\alpha)$. By analogy to the thermal Rossby number $R_T = \Delta_h \alpha$, the parameter $R_E \equiv r\tau\alpha$ can be thought of as a macroturbulent Rossby number, in which the ratio of the thermal and effective eddy-damping time scales replaces differential thermal driving. Since R_T and the inviscid solutions are known, this implies that R_E can be used to predict the value of U_{STJ} for $r > 0$.

A similar dependence on R_E is found for EPTD. The left panel of Fig. 10 shows that in the inviscid case, $EPTD / \Delta_h$ scales with R_T . For $r > 0$, the EPTD, scaled by its respective inviscid EPTD, monotonically decreases with R_E , also reflecting a decrease in available potential energy (not shown).

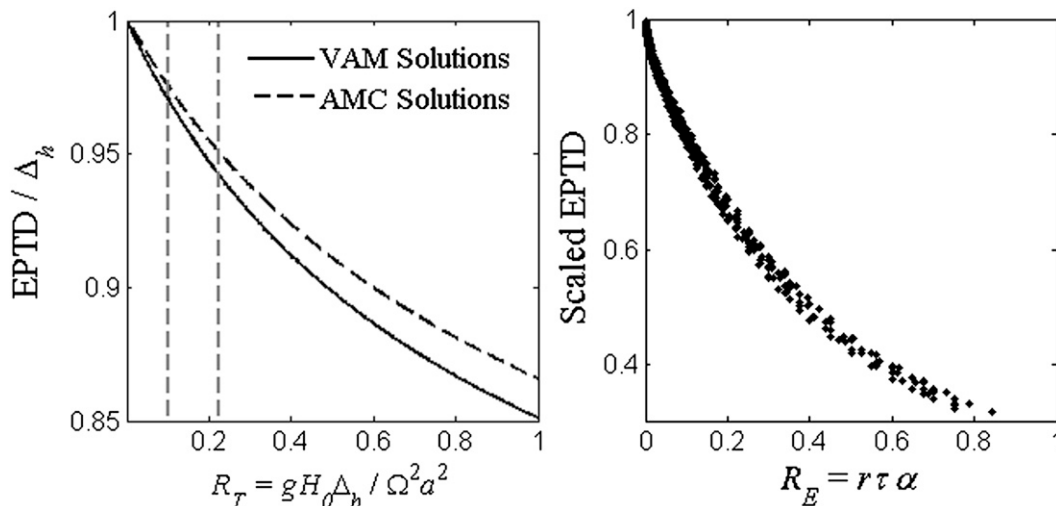


FIG. 10. (left) The dependence of the EPTD divided by the EPTD at Δ_h on R_T in the inviscid case, for VAM (solid) and AMC (dashed) solutions. (right) The dependence of the EPTD of the steady states of the SWM scaled by the respective EPTD in the inviscid case (VAM solutions) on $R_E = r\tau\alpha$. Shown as dots are the values at steady state of the time-dependent SWM obtained by long time integrations for the parameter ranges: $\alpha = 0.15$ – 1.7 , $\Delta_h = 2/15$ – $2/3$ ($R_T = 0.1$ – 0.225), and $r\tau = 0.001$ – 1 . Vertical lines in the left panel indicate the range of R_T values of the viscous steady states shown in the right panel.

The EMFC distribution shown in Fig. 3 has a clear north–south asymmetric component. To examine the effect of asymmetric EMFC, we performed an additional parameter sweep similar to the one described above, in which the value of r was allowed to change per hemisphere, such that

$$r = \begin{cases} r_{\text{NH}}; & \mu > 0 \\ r_{\text{SH}}; & \mu < 0 \end{cases}, \quad (16)$$

where r_{NH} and r_{SH} are positive constants. To avoid instabilities arising from the sharp transition between r_{NH} and r_{SH} , r was smoothed in the vicinity of the equator. The ratio $r_{\text{SH}}/r_{\text{NH}}$ was varied between 1 and 5. Figure 11 shows the dependence on latitude of the meridional (v , dashed), vertical [$w = (Vh)'$, dotted] and zonal (u , gray) winds, and h (solid) at steady state for the symmetric (top panel) and asymmetric case (bottom panel). In both cases $\tau r_{\text{NH}} = 0.006$, $\alpha = 0.45$, and $\Delta_h = 1/3$. The ratio $r_{\text{SH}}/r_{\text{NH}}$ was set to 1 and 3 for the symmetric and asymmetric cases, respectively. The nondimensional vertical wind is given here as $w = (Vh)'$ (cf. Gill 1980), with a scaling of ΩH_0 . For presentational clarity, winds are brought to scale by using units of 100, 0.01, and 10^{-6} m s $^{-1}$, for the zonal, meridional, and vertical winds, respectively. The ascending branch ($w > 0$) is shaded as in Fig. 2.

Since only r is allowed to vary between hemispheres, the ratio $r_{\text{SH}}/r_{\text{NH}}$ also equals the P_r ratio of the two hemispheres. Accordingly, we find that Ro is smaller in the SH, the SH HC strength increases partly at the expense of the

NH HC strength, the ITCZ (the latitude where v changes sign) is shifted toward the NH (3° in Fig. 11b), and the SH subtropical jet is weakened and shifted poleward. We found all of these tendencies to monotonically increase with the $r_{\text{SH}}/r_{\text{NH}}$ ratio. Hemispheric asymmetry in the HC strength and location of the ITCZ comparable to the observed annually averaged atmosphere (Fig. 2) are obtained for $r_{\text{SH}}/r_{\text{NH}} > 3$. Such strong asymmetry in EMFC is not evident in Fig. 3, suggesting that asymmetry in the annually averaged midlatitude total eddy momentum fluxes plays a minor role in determining the asymmetric features of the annually averaged HC.

5. Semianalytic steady solutions for $r > 0$

The findings of the previous section suggest that steady solutions for $r > 0$ possess a strong dependence on the respective inviscid ($r = 0$) solutions. In addition, the deviation from inviscid solutions in general is found to be proportional to the ratio of the thermal and effective eddy forcing time scales $r\tau$ and related to the associated Ro regime. Moreover, from Fig. 5 we find that the “weak eddy-dominance limit” can be defined as

$$P_r = \frac{r\tau}{\alpha\Delta_h^2} = \frac{r\tau\Omega^2 a^2}{gH_0\Delta_h^2} \ll 1. \quad (17)$$

We now proceed to derive the steady solutions for the case of $r > 0$ as deviations from the respective inviscid solutions in the weak eddy-dominance limit. We assume that in this limit, the solutions are small deviations from the

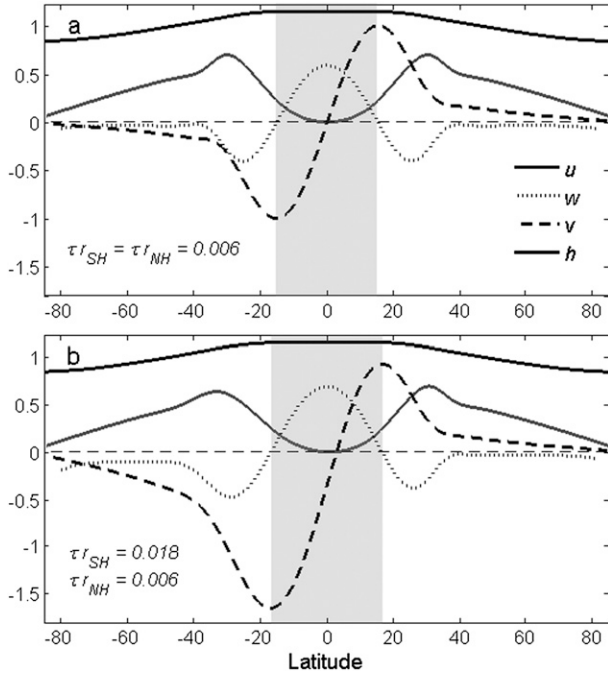


FIG. 11. The dependence on latitude of v (dashed), w (dotted), and u (gray) winds, and h (solid) at steady state for (a) $\alpha = 0.45$, $\Delta_h = 1/3$, and $\tau_{SH} = \tau_{NH} = 0.006$; and (b) $\alpha = 0.45$, $\Delta_h = 1/3$, $\tau_{SH} = 0.018$, and $\tau_{NH} = 0.006$. For presentational clarity, winds are brought to scale by using units of 100, 0.01, and 10^{-6} m s^{-1} , for the zonal, meridional, and vertical winds, respectively. The ascending branch ($w > 0$) is shaded as in Fig. 2. A horizontal zero line (dashed) is added for reference.

inviscid three-region vertical advection of momentum solutions given by Eqs. (4), (5), and (9). For clarity, we shall refer to these regions as the tropical (uniform h , $Q > 0$, in the inviscid case), subtropical (uniform M , $Q < 0$, in the inviscid case), and extratropical (radiative–convective equilibrium in the inviscid case) regions. We use \tilde{V} , \tilde{M} , and \tilde{h} to denote the steady inviscid vertical advection of momentum solutions, and V , M , and h to denote steady-state solutions for $r > 0$. In addition, unless stated otherwise, a scaled variable shall refer to a variable scaled by its respective inviscid value, as in the previous section.

a. Extratropical region

We begin by solving for the functional forms of h , V , and M in the weak eddy-dominance limit at the extratropical region. We note that for $r > 0$, a radiative–convective equilibrium ($V = 0$) steady state does not exist because from Eq. (2b), eddy vorticity fluxes must be balanced by the mean circulation ($M' = \text{absolute vorticity}$). Thus, the SWM is relaxed to a state that is not a steady state of the time-dependent equations. We therefore refer to the extratropical steady state for $r > 0$ as “modified radiative–convective equilibrium.”

Assuming small deviations from inviscid solutions to leading order, the steady form of Eq. (2) becomes

$$M = \frac{\tilde{M}}{2} + \frac{(1 - \mu^2)^2}{2\tilde{M}} \left(1 - \alpha \frac{h'}{\mu} \right) \quad (18a)$$

$$V\tilde{M}' = -r(\tilde{M} - 1 + \mu^2) \quad (18b)$$

$$h = h_f - \tau(Vh_f)', \quad (18c)$$

where from Eq. (5)

$$\tilde{M} = (1 - \mu^2)\sqrt{1 + 2R_T}. \quad (19)$$

We therefore find from Eq. (18b) that

$$V = \frac{r\sqrt{1 + 2R_T} - 1(1 - \mu^2)}{2\sqrt{1 + 2R_T}\mu}. \quad (20a)$$

Using Eq. (18c) we obtain for h , defined as

$$h = h_f + \frac{r\tau\sqrt{1 + 2R_T} - 1}{2\sqrt{1 + 2R_T}} \left[h_f \left(1 + \frac{1}{\mu^2} \right) + 2(1 - \mu^2)\Delta_h \right]. \quad (20b)$$

We then use Eqs. (18a), (19), and (20b) to solve for M , defined as

$$M = (1 - \mu^2) \left[\sqrt{1 + 2R_T} + \frac{3}{2} r\tau\alpha \frac{\sqrt{1 + 2R_T} - 1}{1 + 2R_T} \times \left(\Delta_h + \frac{2 + \Delta_h}{6\mu^4} \right) \right]. \quad (20c)$$

From Eq. (20c), we find that in this region, for small R_T , $U/(\sqrt{1 + 2R_T} - 1)$ scales with $R_E = r\tau\alpha$, as we have found for the subtropical jet maxima of the steady states at long times, shown in Fig. 9.

From Eqs. (5) and (9), the EPTD in the inviscid case is given by $\Delta_h(1 - \mu_A^2)$. Thus, since in the inviscid case μ_A^2 scales with R_T , EPTD/Δ_h also scales with R_T , as shown in the left panel of Fig. 10. Assuming that h remains uniform at the tropics for $r > 0$, from Eq. (20b), for small values of R_T , the EPTD for $r > 0$ is given by

$$\text{EPTD}/\Delta_h = (1 - \mu_A^2) - R_E \left(1 - \frac{1}{2}\Delta_h \right). \quad (21)$$

We therefore find that the scaled EPTD monotonically decreases with R_E , as shown in the right panel of Fig. 10.

b. Tropical region

We now proceed to approximate the functional form of M and h in the tropical region, in which h is assumed

constant (weak temperature gradient approximation). Thus, combining this assumption with steady Eqs. (2b) and (2c) and integrating, we obtain

$$M = 1 - \frac{\int Q \mu^2 d\mu}{\int Q d\mu} - \frac{r\bar{h}}{r\bar{h}} \frac{\int (M - 1 + \mu^2) d\mu}{\int Q d\mu}. \quad (22)$$

We note that in the inviscid case, Eq. (22) is the equivalent of Hide's theorem (cf. HH), that is, $M \leq 1$ everywhere

$$M \simeq 1 - \frac{\mu_A^2 \mu^2 - \frac{3}{5} \mu^4}{3\mu_A^2 - \mu^2} - \frac{r\tau\bar{h}}{\Delta_h} \frac{\frac{2}{5} \mu^2 - \frac{12}{5} \mu_A^2 + \frac{2}{5\mu} (3\mu_A^2)^{3/2} \ln \left(\frac{\sqrt{3}\mu_A + \mu}{\sqrt{3}\mu_A^2 - \mu} \right)}{3\mu_A^2 - \mu^2}, \quad (23a)$$

so that at the polar boundary of this region

$$M(\bar{\mu}) \simeq 1 - \frac{1}{5} \mu_A^2 - \frac{r\tau\bar{h}}{e\Delta_h} \quad (23b)$$

[with $e = \exp(1)$]. The functional form of V in this region is found from Eq. (9) by assuming $h = \bar{h}$ as in the inviscid case.

c. Subtropical region

From Eqs. (23b) and (5), we find that in the inviscid case, the difference in M along the subtropical region, $\Delta M = M(\mu_A) - M(\mu_H)$, is given by

$$\Delta \tilde{M} = 1 - \frac{1}{5} \mu_A^2 - (1 - \mu_H^2) \sqrt{1 + 2R_T}, \quad (24a)$$

and from Eqs. (23b) and (20c), we find for $r > 0$,

$$\begin{aligned} \Delta M = & 1 - \frac{1}{5} \mu_A^2 - \frac{r\tau\bar{h}}{e\Delta_h} \\ & - (1 - \mu_H^2) \left[\sqrt{1 + 2R_T} + \frac{3}{2} r\tau\alpha \frac{\sqrt{1 + 2R_T} - 1}{1 + 2R_T} \right. \\ & \left. \times \left(\Delta_h + \frac{2 + \Delta_h}{6\mu_H^4} \right) \right]. \end{aligned} \quad (24b)$$

Since both μ_A^2 and μ_H^2 scale with R_T , $\Delta \tilde{M}$ also scales with R_T , as shown in the left panel of Fig. 12. By subtracting Eq. (24a) from Eq. (24b), the difference between inviscid and viscous ΔM is given by

$$\begin{aligned} \Delta \tilde{M} - \Delta M = & \frac{r\tau}{\Delta_h} \left[\frac{\bar{h}}{e} + (1 - \mu_H^2) \frac{3}{2} R_T \frac{\sqrt{1 + 2R_T} - 1}{1 + 2R_T} \right. \\ & \left. \times \left(\Delta_h + \frac{2 + \Delta_h}{6\mu_H^4} \right) \right]. \end{aligned} \quad (24c)$$

(Adam and Paldor 2010a). Similarly for $r > 0$, from Eq. (2b) U must vanish where $V = 0$ (cf. Held 2000). This, however, is an intrinsic property of the eddy parameterization of the model rather than a general result applicable to the physical atmosphere (cf. Shell and Held 2004; Sobel and Schneider 2009).

Exact solutions of Eq. (22) for h_f given by Eq. (2d) involve known but unwieldy hypergeometric functions. To avoid unnecessary cumbersome and unrevealing algebra, we assume that $M \simeq \bar{M}$ in the second term on the rhs of Eq. (22) and obtain

Therefore, for small R_T , we expect the relative change in ΔM with respect to the inviscid case, $(\Delta \tilde{M} - \Delta M)/\Delta \tilde{M}$, to scale with $P_r = r\tau/R_T\Delta_h$. The right panel of Fig. 12 shows the log-log dependence of the scaled ΔM on P_r . Unlike the HC strength and region boundaries that possess a dependence on the associated Ro regime, the scaled ΔM exhibits a power-law dependence, $\Delta M/\Delta \tilde{M} \sim \sqrt{P_r}$.

While for $r > 0$ M is continuous everywhere, in the inviscid case M is discontinuous at μ_H (the latitude separating the subtropical angular momentum-conserving region and extratropical radiative convective equilibrium). Therefore, even in the weak eddy-dominance limit, in the vicinity of μ_H deviations from the inviscid solutions of M cannot be regarded as small compared with the inviscid solutions. We therefore make the following heuristic assumption of the functional form of M at the subtropical region:

$$M = \bar{M} - \Delta M [M_1 + M_2 e^{-(1/P_r)(\mu_H^2 - \mu^2)/(1 - \mu^2)}], \quad (25a)$$

where $\bar{M} = M(\mu_A)$ [given by Eq. (23b)], and M_1 and M_2 are constants set to satisfy the boundary conditions $M(\mu_A) = \bar{M}$ and $M(\mu_H) = \bar{M} - \Delta M$, defined as

$$\begin{aligned} M_1 = & -\frac{1}{e^{(1/P_r)(\mu_H^2 - \mu_A^2)/(1 - \mu_A^2)} - 1}; \\ M_2 = & \frac{1}{1 - e^{-(1/P_r)(\mu_H^2 - \mu_A^2)/(1 - \mu_A^2)}}. \end{aligned} \quad (25b)$$

This functional form of M was chosen because it possesses the following properties: (i) it allows a smooth transition from continuous viscous solutions of M to discontinuous inviscid solutions; (ii) in the weak eddy-dominance limit, $P_r \ll 1$, M given by Eq. (25) behaves

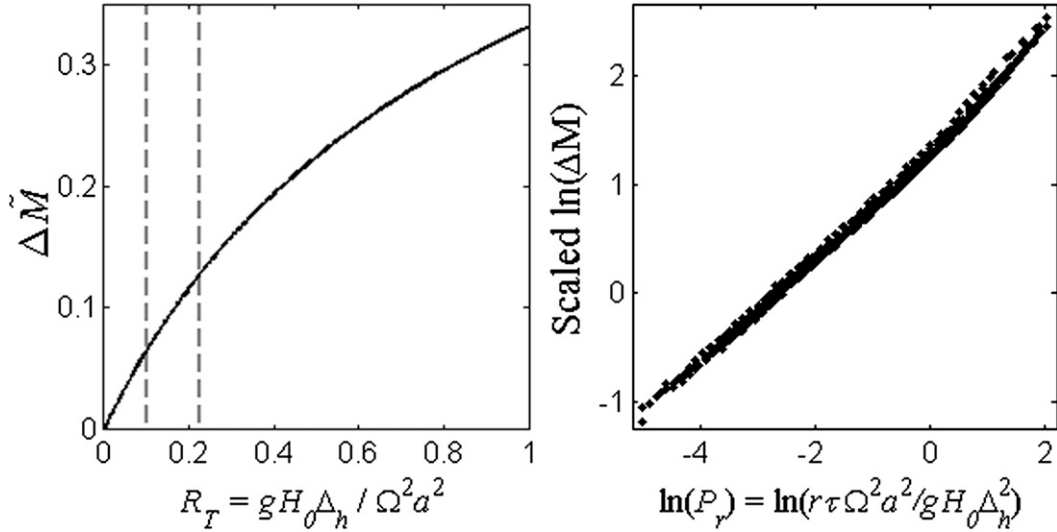


FIG. 12. (left) The dependence of the change in angular momentum along the subtropical region [$\Delta M = M(\mu_A) - M(\mu_H)$], on R_T in the inviscid case (VAM solutions). (right) The log–log dependence of ΔM , scaled by its respective value in the inviscid case on $P_r = r\tau/\Delta_h R_T$. Shown as dots are the values at steady state of the time-dependent SWM obtained by long time integrations for the parameter ranges: $\alpha = 0.15\text{--}1.7$, $\Delta_h = 2/15\text{--}2/3$ ($R_T = 0.1\text{--}0.225$), and $r\tau = 0.001\text{--}1$. As in Fig. 7, steady states for which $\mu_H = 1$, indicating a three-region separation cannot be assumed, are removed from the plot. Vertical lines in the left panel indicate the range of R_T values of the viscous steady states shown in the right panel.

like a small deviation from the value of M in the inviscid case everywhere except near μ_H ; and (iii) it has a finite known integral, allowing us to integrate Eq. (2a) and obtain an expression for h .

We now use Eq. (25) to integrate Eq. (2a) and find to leading order,

$$h \simeq h_0 + \frac{1}{2\alpha} \left[\mu^2 - \frac{\overline{M}^2 - 2M_1 \overline{M} \Delta M}{1 - \mu^2} + 2\overline{M} \Delta M P_r \frac{M_2 e^{-(1/P_r)(\mu_H^2 - \mu^2)/(1 - \mu^2)}}{1 - \mu_H^2} \right], \quad (26)$$

where h_0 is a constant of integration. Finally, V is found from

$$V = \frac{\int (h_f - h) d\mu}{h}. \quad (27)$$

We have now obtained expressions for M , V , and h at the tropics, subtropics, and the extratropics. These expressions depend on the constants μ_H , μ_A , h_0 , \overline{h} , and \overline{M} . To solve for μ_H , μ_A , h_0 , \overline{h} , and \overline{M} , we impose the continuity of M , V , and h at the regions' boundaries and conservation of mass, yielding a set of five equations, which we solve semianalytically. Explicit derivation of the solutions of the five equations is found in the appendix.

Figure 13 shows the functional forms of v (left) and u (right) for steady states at long time integrations of Eq. (2) (thick solid), the weak eddy-dominance semianalytic solutions (thick dashed), vertical advection of momentum (thin solid), and angular momentum–conserving (thin dotted) solutions for $P_r = 0.133$, which we find relevant for present climate conditions. Dashed vertical lines mark the region boundaries. We find that the weak eddy-dominance solutions for u deviate from the solutions at long times in the vicinity of the subtropical jet maxima, but they approximate u well elsewhere. The weak eddy-dominance solutions also overestimate the meridional wind, reflecting an underestimation of the height at the tropics.

Figure 14 shows the convergence of the weak eddy-dominance solutions (dashed) to the steady solutions at long times (solid). Weak eddy-dominance solutions, derived from the roots of Eqs. (A7) and (A8) in the appendix, for $R_T = 0.113$, $\Delta_h = 1/3$ (as in Fig. 13), and $P_r < 1$ are shown for μ_A and μ_{STJ} (top left), subtropical jet amplitude (top right), circulation strength (bottom left), and EPTD (bottom right).

A note on how the semianalytic solutions of the weak eddy-dominance solutions are obtained is in order. The weak eddy-dominance solutions involve nonlinear and transcendental terms whose roots may not be unique. We find that the roots obtained for $P_r \leq 1$ shown in Fig. 14 are unique in the sense that they provide the only

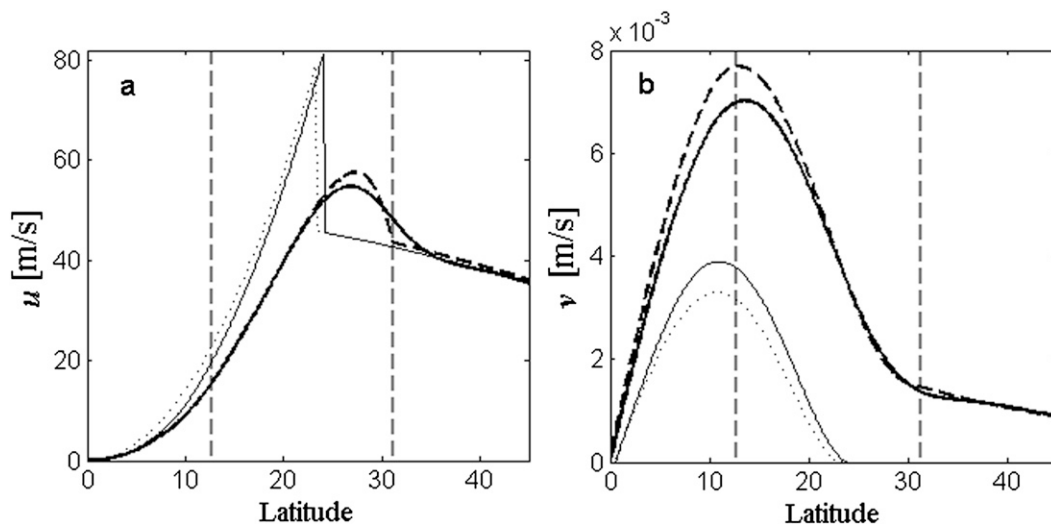


FIG. 13. The dependence on latitude of the steady solutions of (a) u and (b) v for AMC solutions (thin dotted), VAM solutions (thin solid), weak eddy-dominance solutions (thick dashed), and long time integrations of Eq. (2) (thick solid). For presentational clarity, latitudes are truncated at 45° . Vertical dashed lines mark the borders of the subtropical region. Results are shown for a thermal Rossby number, $R_T = 0.113$, $\Delta_h = 1/3$, and $r\tau = 0.005$ ($P_r = 0.133$).

solutions with smooth dependence on P_r . We do not present solutions for $P_r > 1$, as the assumption that the solutions are small deviations from the inviscid three-region structure may not be valid in this case.

6. Summary and discussion

Our aim was to gain qualitative understanding of the interaction of midlatitude eddies with the mean Hadley circulation (HC). In particular, we examined the response of the HC strength and width, the latitude (μ_{STJ}) and amplitude (U_{STJ}) of the subtropical jets, the boundary of the ascending branch of the HC (μ_A), the equator-to-pole temperature difference (EPTD), and the local Rossby number (Ro) to variations in heating and eddy strength.

For this purpose we employed a shallow-water model (SWM) on the rotating Earth to model the upper branch of the HC, forced by annually averaged heating, in which eddies are parameterized as Rayleigh damping r . The rationale for this form of eddy parameterization is twofold: (i) as shown in Fig. 3, eddy momentum flux convergence is approximately proportional to the observed zonally and annually averaged zonal wind at midlatitudes; and (ii) Rayleigh damping provides a simple representation of eddies, allowing analytic insight of the qualitative effect of midlatitude eddies on the HC.

The simplistic shallow-water model and eddy parameterization do not account for extratropical eddy-driven jets, which decouple from the subtropical jets in a

nontrivial manner (e.g., Son and Lee 2005). In addition, the physical interpretation of r is not clear, in particular since the typical damping time of r ($\sim 10^3$ days) cannot be directly related to typical eddy-mean flow response times, which are on the order of a week. This work therefore relates to the macroturbulent HC, with limited relevance to midlatitude dynamics or the general circulation of the atmosphere.

The ascent region and midlatitude eddy response to heating is known to vary between dry and moist models. However, since the only simplifying assumption used here is that eddy damping is proportional to the mean zonal wind, we expect the robust conclusions of this work to equally apply to moist and dry models.

We performed a wide parameter sweep of the steady states of the time-dependent equations [Eqs. (2)] at long times for physically realistic values of the model parameters: α , a planetary Burger's number; Δ_h , the scaled equator-to-pole temperature difference at radiative-convective equilibrium; and $r\tau$, the product of the Rayleigh coefficient of damping and thermal relaxation time.

We find that, for the range of model parameter we examined, an effective HC Prandtl number, which we define as $P_r = \Omega^2 a^2 r\tau / gH_0 \Delta_h^2 = r\tau / \alpha \Delta_h^2 = r\tau / R_T \Delta_h$, nonlinearly predicts the degree of relative dominance of eddy momentum and heat fluxes over the mean HC, exhibiting distinct regimes of weak ($\text{Ro} \sim 1$), intermediate ($0 < \text{Ro} < 1$), and strong ($\text{Ro} \sim 0$) eddy dominance (Fig. 5). We estimate $P_r \sim 0.13$ for Earth's present climate.

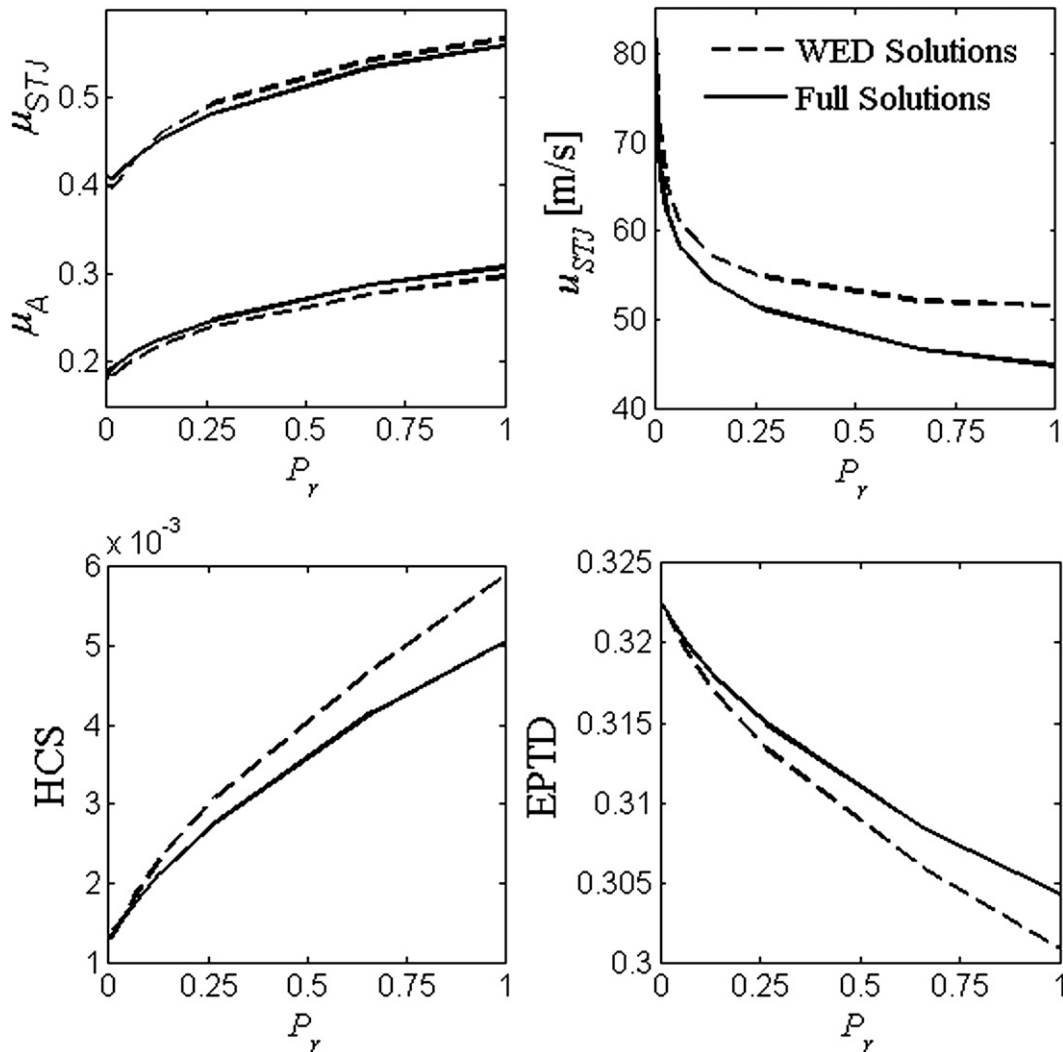


FIG. 14. The dependence on $P_r = r\tau/\Delta_h R_T$ of the steady states at long times (full solutions, solid) and weak eddy-dominance semianalytic (WED, dashed) solutions obtained from the roots of Eqs. (A7) and (A8) for $R_T = 0.113$ and $\Delta_h = 1/3$, as in Fig. 13. Results are shown for (top left) μ_{STJ} and μ_A , (top right) u_{STJ} , (bottom left) $HCS = \max(Vh)$, and (bottom right) EPTD.

We also find that P_r approximately predicts the relative deviation from inviscid solutions for the boundary of the ascending branch (Fig. 8), HC strength (Fig. 7), width (Fig. 8), and change in angular momentum along the subtropics (Fig. 11). Similarly, the relative change of the subtropical jet strength and equator-to-pole temperature difference from their respective inviscid solutions are found to scale with $R_E = r\tau\alpha$ (Figs. 9 and 10, respectively), which we term here as a macroturbulent Rossby number, analogous to the thermal Rossby number $R_T = \Delta_h\alpha$.

Turning to Fig. 5, we find that P_r predicts a weakening of the relative dominance of eddies (i.e., increased Ro) in response to increased mean temperature (H_0, α), in

accordance with the response found in more complex models (e.g., Levine and Schneider 2011). Similarly, since the equator-to-pole temperature difference at radiative-convective equilibrium is smaller in the summer hemisphere, P_r predicts that eddies are more dominant in the summer hemisphere than in the winter hemisphere, in accordance with more complex models as well as the observed atmosphere (e.g., Walker and Schneider 2006; Schneider and Bordoni 2008). From Figs. 7 and 8 we see that inviscid theory predicts a monotonic increase in HC strength and width in response to mean (α) or differential (Δ_h) heating. From Fig. 7, we deduce that a decrease in the HC strength in response to heating can occur only at intermediate or strong eddy dominance,

and only if the eddy component of the HC decreases in response to the heating. These conditions are consistent with the nonmonotonic HC strength response to heating found by Levine and Schneider (2011).

To test the effect of equatorially asymmetric eddy damping (as opposed to equatorially asymmetric heating), we performed an additional parameter sweep in which a different value of r was used for each hemisphere. For Southern Hemisphere r (r_{SH}) greater than r at the Northern Hemisphere (r_{NH}), we found that (i) the SH HC strength increased partly at the expense of the NH HC strength; (ii) the ITCZ (the latitude where ν changes sign) was shifted to the north; and (iii) the SH subtropical jet was damped and shifted poleward. These tendencies increased monotonically with increasing $r_{\text{SH}}/r_{\text{NH}}$ ratios. Hadley circulation strength and ITCZ shift comparable to those observed in the atmosphere (Fig. 2) were obtained for $r_{\text{SH}}/r_{\text{NH}} > 3$. Such strong asymmetry, however, is not observed in the annually averaged EMFC (Fig. 3), suggesting that this simplified asymmetry plays a minor role in determining the asymmetric properties of the annually averaged HC.

From Figs. 7–10 we learn that the relative deviation of the steady states of the viscous HC is strongly dependent on the values of P_r and R_E , as well as on the associated Ro regime. We thus define the “weak eddy-dominance limit” as $P_r \ll 1$.

In the inviscid case, inviscid solutions follow a three-region paradigm: weak temperature gradient at the ascending branch of the HC, angular momentum conservation at the descending branch, and radiative–convective equilibrium at the extratropics. We derived semianalytic solutions of the SWM in the weak eddy-dominance limit by assuming that for sufficiently low values of P_r , the three-region paradigm, which dominates the inviscid solutions, can be applied to the eddy-permitting HC. Solutions are derived as small deviations from the known three-region inviscid steady states. The modified three regions are: weak temperature gradient at the ascending branch, a smooth monotonically decreasing angular momentum at subtropics [Eq. (25)], and modified radiative–convective equilibrium at the extratropics.

Approximate expressions for the modified steady states in the weak eddy-dominance limit are derived and solved semianalytically in section 5. These expressions yield the scaling relations found in the parameter sweep of the model for the steady-state HC strength (Fig. 7) and width

(Fig. 8), the boundary of the ascending branch (Fig. 8), subtropical jet strength (Fig. 9), equator-to-pole temperature difference (Fig. 10), and the change in angular momentum along the subtropics (Fig. 12). The weak eddy-dominance solutions diverge from the time-dependent solutions at long times as P_r increases and may be invalid for $P_r > 1$.

The weak eddy-dominance solutions can be extended to other forms of eddy parameterization, potentially more realistic than Rayleigh damping, which may better capture seasonal climatology. A simple parameterization of the gross response of eddies to variations of external parameters, for example, $r(\alpha, \Delta_h)$, may further elucidate the nonlinear interaction of midlatitude eddies and the mean HC.

Our findings suggest that in the intermediate regime of eddy dominance, the properties of the HC are determined by a base three-region inviscid state, given by R_T and Δ_h , and a deviation from that state, predicted by P_r . The steady states of the idealized model are found to be in agreement with more complex models as well as the observed atmosphere. Thus, the idealized macro-turbulent HC SWM provides powerful insight into the interaction of the HC and midlatitude eddies. Given the simplicity and qualitative agreement of the model with more complex models as well as the observed atmosphere, the weak eddy-dominance solutions may therefore be regarded as a meaningful step toward a theory of the macro-turbulent HC in the intermediate eddy-dominance regime.

Acknowledgments. We wish to thank Nathan Paldor, Eyal Heifetz, Yair Cohen, and Jian Lu for their useful comments and advice during the inception and preparation of this work. We also thank Isaac Held and an anonymous reviewer for their instructive suggestions. This study was partly funded by TAU Council of Higher Education and partly by the Israeli Science Foundation Grant 1370/08.

APPENDIX

Semianalytic Solutions of the SWM

Neglecting terms proportional to V and substituting Eq. (24) into steady Eq. (2), we find

$$h' \simeq \frac{\mu}{\alpha} \left[1 - \frac{\bar{M}^2 + M_1^2 \Delta M^2 - 2\bar{M}M_1 \Delta M - 2M_2 \Delta M (\bar{M} - M_1 \Delta M) e^{-(1/P_r)(\mu_h^2 - \mu^2)(1 - \mu^2)} + \Delta M^2 M_2^2 e^{-(2/P_r)(\mu_h^2 - \mu^2)(1 - \mu^2)}}{(1 - \mu^2)^2} \right] \quad (\text{A1})$$

so that to leading order, in the midregion

$$h \simeq h_0 + \frac{1}{2\alpha} \left[\mu^2 - \frac{\overline{M}^2 - 2M_1\overline{M}\Delta M}{1 - \mu^2} + 2\overline{M}\Delta MP_r \frac{M_2 e^{-(1/P_r)(\mu_H^2 - \mu^2)/(1 - \mu^2)}}{1 - \mu_H^2} \right]. \tag{A2}$$

Now that the functional forms of M , V , and h are known in the three regions, we proceed to write the equations for μ_A , μ_H , \bar{h} , \overline{M} , and h_0 for $r > 0$ by imposing the continuity of h and M and the conservation of mass. Mass conservation yields

$$\int_0^{\mu_A} (h_f - \bar{h}) d\mu + \int_{\mu_A}^{\mu_H} \left\{ h_f - h_0 - \frac{1}{2\alpha} \left[\mu^2 - \frac{\overline{M}^2 - 2M_1\overline{M}\Delta M}{1 - \mu^2} + \overline{M}\Delta MP_r \frac{M_2 e^{-(1/P_r)(\mu_H^2 - \mu^2)/(1 - \mu^2)}}{1 - \mu_H^2} \right] \right\} d\mu - \int_{\mu_H}^1 \frac{r\sqrt{1+2R_T}-1}{2\sqrt{1+2R_T}} \left[h_f \left(1 + \frac{1}{\mu^2} \right) + (1 - \mu^2)2\Delta_h \right] d\mu = 0. \tag{A3}$$

Imposing continuity at μ_A , we obtain

$$\bar{h} = h_f(\mu_A) = 1 + \Delta_h \left(\frac{1}{2} - \mu_A^2 \right) \tag{A4}$$

and

$$h_0 + \frac{1}{2\alpha} \left[\mu_A^2 - \frac{\overline{M}^2 - 2M_1\overline{M}\Delta M}{1 - \mu_A^2} + \frac{2\overline{M}M_2\Delta MP_r e^{-(1/P_r)(\mu_H^2 - \mu_A^2)/(1 - \mu_A^2)}}{(1 - \mu_H^2)} \right] = h_f(\mu_A) = 1 + \Delta_h \left(\frac{1}{2} - \mu_A^2 \right) \tag{A5}$$

and from continuity at μ_H we obtain

$$h_0 + \frac{1}{2\alpha} \left(\mu_H^2 - \frac{\overline{M}^2 - 2M_1\overline{M}\Delta M - 2\overline{M}M_2\Delta MP_r}{1 - \mu_H^2} \right) = h_f(\mu_H) + \frac{r\sqrt{1+2R_T}-1}{2\sqrt{1+2R_T}} \left[h_f(\mu_H) \left(1 + \frac{1}{\mu_H^2} \right) + (1 - \mu_H^2)2\Delta_h \right]. \tag{A6}$$

By setting \bar{h} from continuity at μ_A [Eq. (A4)], h_0 from continuity at μ_H [Eq. (A6)], using Eqs. (23b) and (24) for \overline{M} and ΔM , respectively, and neglecting the contribution of the exponential terms to the integral in Eq. (A3), Eqs. (A3)–(A6) are reduced to

$$(\mu_H^2 - \mu_A^2) \left[1 + 2R_T - \frac{\overline{M}^2 - 2M_1\overline{M}\Delta M}{(1 - \mu_H^2)(1 - \mu_A^2)} \right] + 2M_2\overline{M}\Delta MP_r \frac{1 - e^{-(1/P_r)(\mu_H^2 - \mu_A^2)/(1 - \mu_A^2)}}{1 - \mu_H^2} = \alpha r \frac{\sqrt{1+2R_T}-1}{\sqrt{1+2R_T}} \left(1 + \frac{3}{2}\Delta_h - 3\Delta_h\mu_H^2 + \frac{1 + \frac{1}{2}\Delta_h}{\mu_H^2} \right) \tag{A7}$$

and

$$\frac{4R_T}{3}\mu_A^3 + (1 + 2R_T) \left(\frac{2}{3}\mu_H^3 + \frac{1}{3}\mu_A^3 - \mu_H^2\mu_A \right) + (\overline{M}^2 - 2M_1\overline{M}\Delta M) \left\{ \frac{1}{2} \ln \left[\frac{(1 + \mu_H)(1 - \mu_A)}{(1 - \mu_H)(1 + \mu_A)} \right] - \frac{(\mu_H - \mu_A)}{1 - \mu_H^2} \right\} = \alpha r \frac{\sqrt{1+2R_T}-1}{\sqrt{1+2R_T}} \left[\left(1 + \frac{3}{2}\Delta_h \right) (1 - \mu_A) + \Delta_h (3\mu_H^2\mu_A - 2\mu_H^3 - 1) + \frac{1 + \frac{1}{2}\Delta_h}{\mu_H^2} (2\mu_H - \mu_A - \mu_H^2) \right]. \tag{A8}$$

It is readily verified that by setting $r = 0$, the corresponding inviscid equations for μ_A and μ_H [Eq. (12)] are reproduced. The region boundaries μ_A and μ_H are found as the roots of Eqs. (A7) and (A8), thus setting the values of \bar{M} [Eq. (23)], \bar{h} [Eq. (A4)], and h_0 [Eq. (A2)].

REFERENCES

- Adam, O., and N. Paldor, 2009: Global circulation in an axially symmetric shallow water model forced by equinoctial differential heating. *J. Atmos. Sci.*, **66**, 1418–1433.
- , and —, 2010a: Global circulation in an axially symmetric shallow-water model, forced by off-equatorial differential heating. *J. Atmos. Sci.*, **67**, 1275–1286.
- , and —, 2010b: On the role of viscosity in ideal Hadley circulation models. *Geophys. Res. Lett.*, **37**, L16801, doi:10.1029/2010GL043745.
- Becker, E., G. Schmitz, and R. Geprags, 1997: The feedback of midlatitude waves onto the Hadley cell in a simple general circulation model. *Tellus*, **49A**, 182–199.
- Emanuel, K. A., J. D. Neelin, and C. S. Bretherton, 1994: On large-scale circulations in convecting atmospheres. *Quart. J. Roy. Meteor. Soc.*, **120**, 1111–1143.
- Fang, M., and K. K. Tung, 1996: A simple model of nonlinear Hadley circulation with an ITCZ: Analytic and numerical solutions. *J. Atmos. Sci.*, **53**, 1241–1261.
- , and —, 1997: The dependence of the Hadley circulation on the thermal relaxation time. *J. Atmos. Sci.*, **54**, 1379–1384.
- , and —, 1999: Time-dependent nonlinear Hadley circulation. *J. Atmos. Sci.*, **56**, 1797–1807.
- Gill, A. E., 1980: Some simple solutions of the heat-induced tropical circulation. *Quart. J. Roy. Meteor. Soc.*, **106**, 447–462.
- , 1982: *Atmosphere–Ocean Dynamics*. Academic Press, 662 pp.
- Held, I. M., 2000: The Hadley cell. *Proc. 2000 Program in Geophysical Fluid Dynamics: The General Circulation of the Atmosphere*, Woods Hole, MA, Woods Hole Oceanographic Institution, 39–48. [Available online at <https://www.whoi.edu/fileserver.do?id=21464&pt=10&p=17332>.]
- , and A. Y. Hou, 1980: Nonlinear axially symmetric circulations in a nearly inviscid atmosphere. *J. Atmos. Sci.*, **37**, 515–533.
- , and B. Hoskins, 1985: Large-scale eddies and the general circulation of the troposphere. *Advances in Geophysics*, Vol. 28A, Academic Press, 3–31.
- , and B. J. Soden, 2006: Robust response of the hydrological cycle to global warming. *J. Climate*, **19**, 5686–5699.
- Hou, A. Y., 1984: Axisymmetric circulations forced by heat and momentum sources: A simple model applicable to the Venus atmosphere. *J. Atmos. Sci.*, **41**, 3437–3455.
- , and R. S. Lindzen, 1992: The influence of concentrated heating on the Hadley circulation. *J. Atmos. Sci.*, **49**, 1233–1241.
- Johanson, C., and Q. Fu, 2009: Hadley cell widening: Model simulations versus observations. *J. Climate*, **22**, 2713–2725.
- Kang, S., and J. Lu, 2012: Expansion of the Hadley cell under global warming: Winter versus summer. *J. Climate*, **25**, 8387–8393.
- Kim, H.-Y., and S. Lee, 2001: Hadley cell dynamics in a primitive equation model. Part I: Axisymmetric flow. *J. Atmos. Sci.*, **58**, 2845–2858.
- Lee, S., 1999: Why are the climatological zonal mean winds easterly in the equatorial upper troposphere? *J. Atmos. Sci.*, **56**, 1353–1363.
- Levine, X. J., and T. Schneider, 2011: Response of the Hadley circulation to climate change in an aquaplanet GCM coupled to a simple representation of ocean heat transport. *J. Atmos. Sci.*, **68**, 769–783.
- Lindzen, R. S., and A. Y. Hou, 1988: Hadley circulations for zonally averaged heating centered off the equator. *J. Atmos. Sci.*, **45**, 2416–2427.
- Lorenz, D. J., and D. L. Hartmann, 2001: Eddy–zonal flow feedback in the Southern Hemisphere. *J. Atmos. Sci.*, **58**, 3312–3327.
- Lu, J., G. A. Vecchi, and T. Reichler, 2007: Expansion of the Hadley cell under global warming. *Geophys. Res. Lett.*, **34**, L06805, doi:10.1029/2006GL028443.
- Mitas, C. M., and A. Clement, 2005: Has the Hadley cell been strengthening in recent decades? *Geophys. Res. Lett.*, **32**, L03809, doi:10.1029/2004GL021765.
- Pfeffer, R. L., 1981: Wave-mean flow interactions in the atmosphere. *J. Atmos. Sci.*, **38**, 1340–1359.
- Polvani, L. M., and A. H. Sobel, 2002: The Hadley circulation and the weak temperature gradient approximation. *J. Atmos. Sci.*, **59**, 1744–1752.
- Santer, B. D., and Coauthors, 2005: Amplification of surface temperature trends and variability in the tropical atmosphere. *Science*, **309**, 1551–1556.
- Satoh, M., 1994: Hadley circulations in radiative–convective equilibrium in an axially symmetric atmosphere. *J. Atmos. Sci.*, **51**, 1947–1968.
- Schneider, E. K., 1977: Axially symmetric steady-state models of the basic state for instability and climate studies. Part II: Nonlinear calculations. *J. Atmos. Sci.*, **34**, 280–296.
- , 1984: Response of the annual and zonal mean winds and temperatures to variation in the heat and momentum sources. *J. Atmos. Sci.*, **41**, 1093–1115.
- , 1987: A simplified model of the modified Hadley circulation. *J. Atmos. Sci.*, **44**, 3311–3328.
- Schneider, T., 2006: The general circulation of the atmosphere. *Annu. Rev. Earth Planet. Sci.*, **34**, 655–688.
- , and S. Bordoni, 2008: Eddy-mediated regime transitions in the seasonal cycle of a Hadley circulation and implications for monsoon dynamics. *J. Atmos. Sci.*, **65**, 915–934.
- Shell, K. M., and I. M. Held, 2004: Abrupt transition to strong superrotation in an axisymmetric model of the upper troposphere. *J. Atmos. Sci.*, **61**, 2928–2935.
- Sobel, A. H., and T. Schneider, 2009: Single-layer axisymmetric model for a Hadley circulation with parameterized eddy momentum forcing. *J. Adv. Model. Earth Syst.*, **1**, doi:10.3894/JAMES.2009.1.10.
- , J. Nilsson, and L. M. Polvani, 2001: The weak temperature gradient approximation and balanced tropical moisture waves. *J. Atmos. Sci.*, **58**, 3650–3665.
- Son, S. W., and S. Lee, 2005: The response of westerly jets to thermal driving in a primitive equation model. *J. Atmos. Sci.*, **62**, 3741–3757.
- Walker, C. C., and T. Schneider, 2006: Eddy influences on Hadley circulations: Simulations with an idealized GCM. *J. Atmos. Sci.*, **63**, 3333–3350.